Hindawi Publishing Corporation
International Journal of Photoenergy
Volume 2014, Article ID 149520, 8 pages
http://dx.doi.org/10.1155/2014/149520

Research Article

Bottom-Up Enhancement of g-C_3N_4 Photocatalytic H_2 Evolution Utilising Disordering Intermolecular Interactions of Precursor

Xue Lu Wang,[1,2] Wen Qi Fang,[1] Yu Hang Li,[1] Pengfei Liu,[1] Haimin Zhang,[2] Yun Wang,[2] Porun Liu,[2] Yefeng Yao,[3] Huijun Zhao,[2] and Hua Gui Yang[1,2]

[1] *Key Laboratory for Ultrafine Materials of Ministry of Education, School of Materials Science and Engineering, East China University of Science and Technology, 130 Meilong Road, Shanghai 200237, China*
[2] *Centre for Clean Environment and Energy, Griffith University, Gold Coast Campus, Gold Coast, QLD 4222, Australia*
[3] *Physics Department and Shanghai Key Laboratory of Magnetic Resonance, East China Normal University, Shanghai 200062, China*

Correspondence should be addressed to Huijun Zhao; h.zhao@griffith.edu.au and Hua Gui Yang; hgyang@ecust.edu.cn

Received 9 June 2014; Revised 20 August 2014; Accepted 8 September 2014; Published 30 November 2014

Academic Editor: Wenjun Luo

Disordered intermolecular interaction carbon nitride precursor prepared by water-assisted grinding of dicyandiamide was used for synthesis of g-C_3N_4. The final sample possesses much looser structure and provides a broadening optical window for effective light harvesting and charge separation efficiency, which exhibits significantly improved H_2 evolution by photocatalytic water splitting. The bottom-up mechanochemistry method opens new vistas towards the potential applications of weak interactions in the photocatalysis field and may also stimulate novel ideas completely different from traditional ones for the design and optimization of photocatalysts.

1. Introduction

Spurred by the increasing global energy demands and environmental issues, a noble pathway for converting solar energy into clean fuels has been widely recognised. Among various types of solar energy conversion, solar chemical conversion such as photolysis of water into hydrogen (H_2) has been regarded as a promising way to transfer biological photosynthesis to a manmade environment with a higher efficiency than plants [1, 2]. Thus, considerable efforts have been devoted to exploring robust photocatalytic systems for the purpose of efficient absorption, utilization, and conversion of solar photons in a sustainable manner [3, 4]. However, low light utilisation efficiency and high recombination of photogenerated carriers in most photocatalytic systems limit the applicability of photocatalysts for large-scale H_2 photosynthesis. Recently, organic polymer or supermolecular systems, which are much closer to the nature plant, have been introduced as solar-photons transducers and stimulated continuous research attentions [5, 6].

Polymeric graphitic carbon nitride (g-C_3N_4), a simple, efficient, highly stable, and sustainable organic material, has been introduced as a metal-free visible light photocatalyst for water splitting and attracted worldwide renaissance attention [4]. To improve the photocatalytic activities of g-C_3N_4, several strategies have been developed, such as doping [7–10], templating [11–13], cocatalyzing [14, 15], copolymerization [16, 17], heterogeneous catalysis [18, 19], and surface modification [20, 21]. In general, bulk g-C_3N_4 was synthesized by pyrolysis of nitrogen-rich organic precursors, such as cyanamide [4], dicyandiamide [14], melamine [11], ammonium thiocyanate [22], urea [23], and thiourea [24]. Nevertheless, most of the precursors involved in the synthetic process are crystallographic materials, and researchers considered only structures and functions involving strong covalent bonds. Instead, the structures of these organic precursors are usually made from loose aggregates that are held together by weak, noncovalent interactions, which are responsible for most of the processes occurring in living systems because of their dynamic nature [25–27]. As we

know, mechanochemical reaction such as ball mill grinding can break up the materials to expose fresh surfaces, introduce various defects, and eventually result in amorphization [28]. The crystal structures of organic solids which are very different in many respects from inorganic materials especially are usually anisotropic, and the shapes and the intermolecular interactions of organic particles are far from being isometric and different crystal faces have different properties [28]. Thus, new routes for the synthesis of compounds will be opened if we preprocess the precursors by mechanical action.

Herein, we for the first time developed a bottom-up strategy to synthesize g-C_3N_4 photocatalysts with improved optical property and chemical structure through using disordered dicyandiamide (D-DCDA) as reaction precursor. The D-DCDA was obtained by water-assisted grinding (WAG) of crystallographic dicyandiamide (DCDA). The final carbon nitride sample (D-CN) condensed by D-DCDA possesses much looser structure and provides a broadening optical window for effective light harvesting and charge separation efficiency which results in the significant enhancement in photocatalytic activity for hydrogen evolution.

2. Material and Methods

2.1. Materials Synthesis. The D-DCDA precursor was carried out in a planetary ball-mill machine (QM-3SP2) in the presence of deionized (DI) water. In a typical fabrication, 2 g of DCDA powders was added into an agate capsule containing agate balls of 5 mm in diameter. 10 mL of DI water was added into the above capsule as solvents assisted grinding. The container was fixed in the planetary ball-mill machine and agitated with 300 rpm for 12 h. The result products were collected by centrifugation with DI water and dried at 80°C under vacuum for 24 h.

The D-CN sample was prepared by a facile thermal treatment of D-DCDA. Typically, 1 g of the as-prepared D-DCDA power was put into a covered crucible and then heated at a rate of 5°C min^{-1} to reach the temperature of 550°C and maintained at this temperature in air for 2 h. The samples obtained by simply heating DCDA at 550°C were denoted by CN and were used as a reference sample.

2.2. Methods. The structures of the power samples were investigated by X-ray diffractometer (XRD, Bruker D8 Advanced Diffractometer operating with Cu Kα radiation). The angular range was 2θ = 5–75°, with a speed of 6°/min. Infrared transmission was obtained with a Fourier transform infrared (FTIR) spectrophotometer Spectrum (Nicolet). The optical absorbance spectra of the samples were performed on using a UV-vis spectrometer (CARY 300). All binding energies were referenced to C1s peaks (284.8 eV) arising from surface hydrocarbons (or possible adventitious hydrocarbon). Element analysis was conducted by an elemental analyzer (vario ELII; Elementar Analysensyteme, Germany). The photoluminescence measurements were performed in an Edinburgh instruments (FLSP 920) system operated at room temperature. The carbon and nitrogen K-edge X-ray absorption near-edge structure (XANES) measurement of the samples were performed at the beamline 4B7B of Beijing Synchrotron Radiation Facility (BSRF). Brunauer-Emmett-Teller (BET) surface areas were determined by a TriStar 3020 nitrogen sorption isotherm apparatus.

3. Results

The possible mechanism diagrams of the synthesis of D-DCDA and D-CN are illustrated in Figure 1(a). After ball milling DCDA in the presence of deionized water, the parking patterns of the crystal structure of DCDA molecules become disordered owing to the introduction of water molecules by the stronger hydrogen bond [29, 30]. Chemical structures of D-DCDA were characterized with various techniques such as XRD, FTIR, and solid-state NMR. Figure 1(b) exhibits the XRD patterns of the DCDA and D-DCDA samples. The position of the main peaks of the two samples is almost same. However, the intensities of peaks sharply decrease after WAG of the DCDA, which indicates the deterioration of crystallinity which led to the destroyed molecules framework or disordered arrangement of molecules units. More structural properties of the D-DCDA were further characterized by SEM, FTIR and ^{13}C solid-state NMR measurements. As can be seen from Figure S1, (see Figure S1 at Supplementary Material available online at http://dx.doi.org/10.1155/2014/149520) after the ball milling treatment, the particle size of DCDA decreased to about 1/10 of the original one. Figure 1(c) and S2 show that the FTIR and NMR spectra of the D-DCDA and DCDA are similar, suggesting that the composition monomer units of the D-DCDA remain unchanged compared with those of the DCDA. Thus, the possible destruction of surface functional groups and the covalent intramolecular bonds can be ruled out.

In order to understand the possible reaction process during pyrolysis of DCDA and D-DCDA, TG and DSC were carried out. As can be seen from the mass-loss curve (Figure 1(d)), most activities occur in the range of 210–720°C. For D-DCDA, a slowed weight loss tendency is observed, which can be assigned to the less sublimation and evaporation of some small molecules derived from the pyrolysis; that is, more molecules are involved in the real reaction progress [31]. In addition, there is still 6.48 wt.% of residuals above 700°C for D-DCDA, which would be due to the formation of stable C species at high temperature [32, 33]. Therefore, the final product D-CN may exist as some nitrogen defect or structure distortion compared to the CN sample. Figure 1(e) shows the DSC curves of the two precursors. An endothermic peak at around 213°C is the melting point of them [34]. However, it seems that D-DCDA has the lower melting point. Ordinary, melting-point depression is the phenomenon of reduction of the melting point of a material with reduction of its size, which is accompanied with some lattice distortion. These accord well with the results obtained by XRD. Subsequently, the first strong exothermic peak is at about 237°C, which indicated that sample starts to decompose and aggregate into melamine [4, 31]. Interestingly, another new exothermic peak appears at 255°C for the D-DCDA, which means D-DCDA undergoing two exothermic reactions during the formation

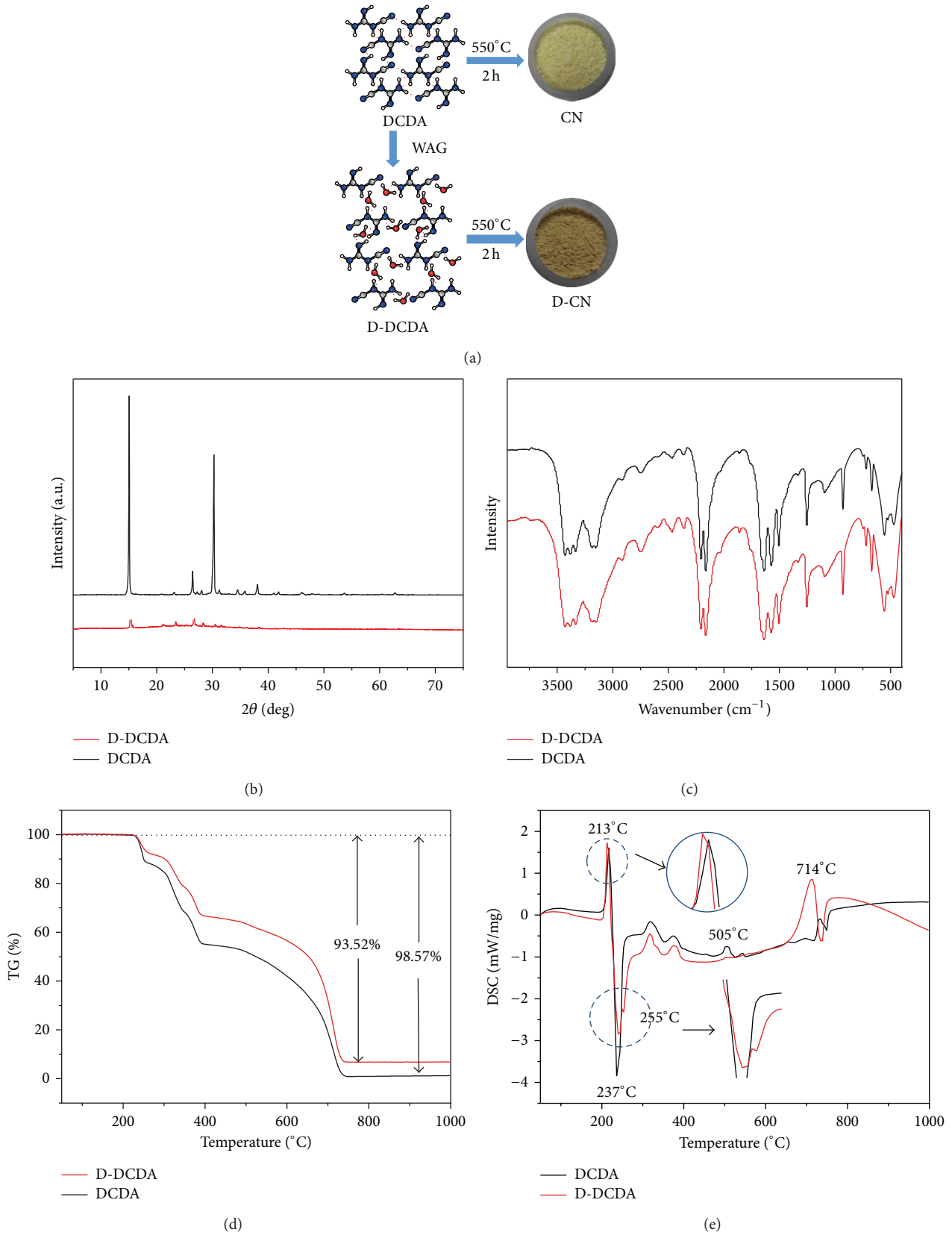

Figure 1: (a) Schematic illustration for the synthesis process of CN and D-CN. (b) XRD patterns, (c) FTIR spectra, (d) TG curves, and (e) DSC curves of the DCDA and D-DCDA samples.

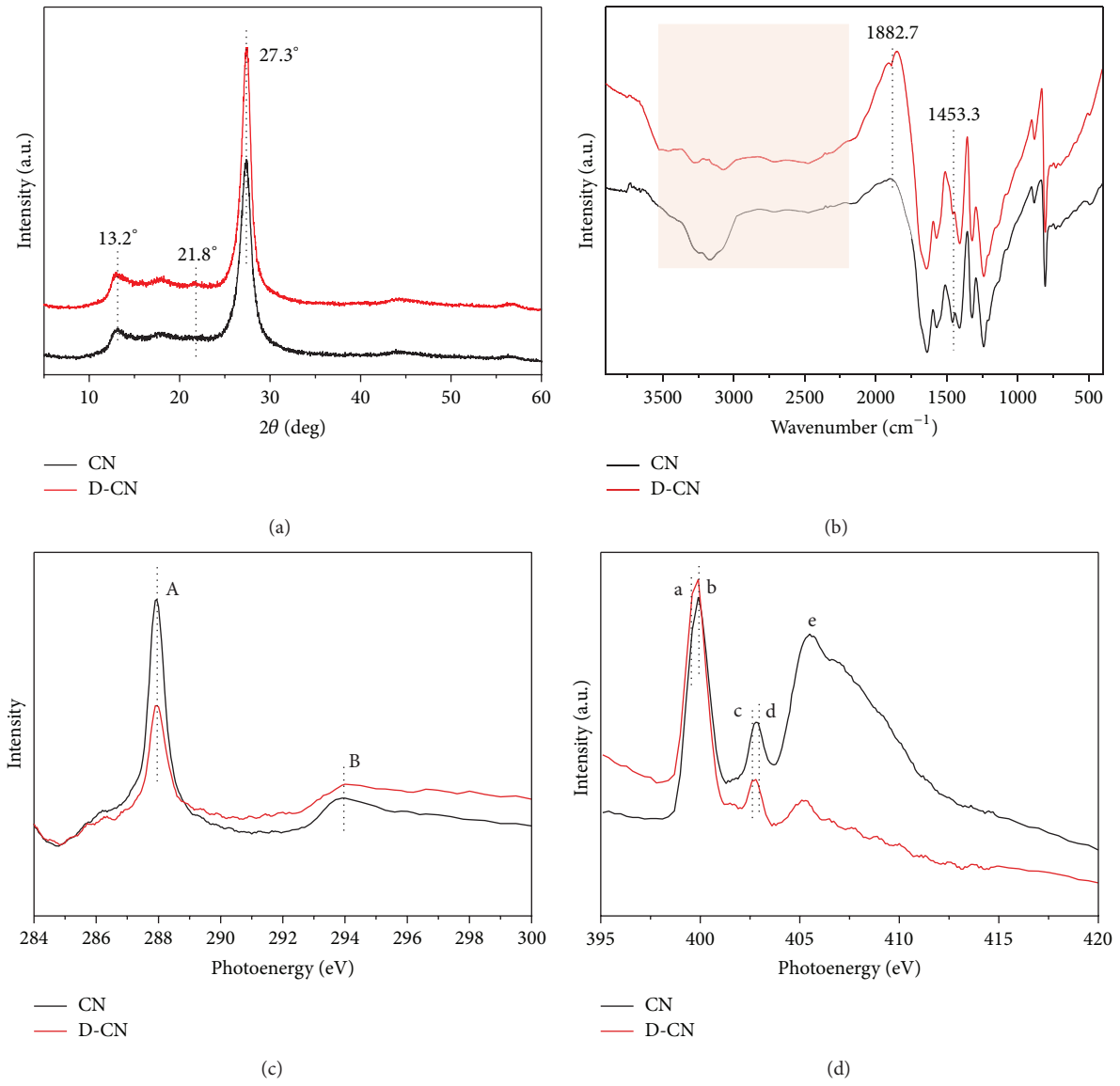

Figure 2: Comparison of XRD patterns (a), FTIR spectra (b), C K-edge (c), and N K-edge (d) XANES spectra of CN and D-CN.

of melamine, leading to the different degrees of condensation and different packing motifs. Finally, the endothermic peak at 714°C can be attributed to the sublimation of carbon nitride [31, 34]. The earlier decomposition point for D-DCDA further proves the incomplete structure.

To shed light on the effect of disordering of precursors on the performance of the final g-C_3N_4 products, various characterizations have been conducted. The carbon and nitrogen stoichiometry of prepared samples were determined by elemental analysis. As shown in Table S1, the C/N atomic ratio of the D-CN was determined as 0.676, which is very close to the bulk CN (0.675) but lower than that of the theoretical value of the ideal crystal g-C_3N_4 (0.75). Trace amounts of other compositions may be caused by absorbed H_2O and substituted oxygen. The XRD patterns of CN and D-CN samples are quite similar, which represent their graphitic like structures stacked by tri-s-triazine based connection sheet as units. They all show two feature diffraction peaks at around 13.2° and 27.3°, characteristic of the interplanar structural repeating motifs and the stacking peak of conjugated aromatic systems, respectively [4]. However, a small new peak appears at 21.8° for D-CN and may originate from the defective condensation of melon structures [5].

The bonding of carbon and nitrogen of the final samples was analysed through FTIR spectra (Figure 2(b)). In the case of bulk CN, the set of peaks between 1700 and 1200 cm^{-1} is characteristic of organic molecules containing tri-s-triazine ring moieties, while the sharp peak at around 810 cm^{-1} is considered as their breathing mode. Additionally, the absorbance in the region of 3000–3500 cm^{-1} is assignable to the presence of secondary and primary amines and the O–H band which is originated from the uncondensed amino groups and adsorbed H_2O molecules, respectively. The obvious widen tendency of D-CN also implies the defective condensation.

In addition, besides the similar skeleton signs, some minute distinctions can be observed on the D-CN sample. To be specific, the peak at around 1453 cm^{-1} which is attributable to a network structure of triazine rings cross-linked with NH end and >N-groups becomes weak and less developed [18, 20]. A small peak of D-CN at around 1883 cm^{-1} may be related to the C=O stretching induced by unavoidable oxidation from the D-DCDA. All these observations speak for the formation of a more defected polymeric network of g-C_3N_4 for D-CN compared to CN.

The chemical structures of the samples were further analysed by XPS measurements. The C1s spectra in Figure S3A can be deconvoluted into three peaks at 284.7, 288.2, and 289.4 eV, which are assigned to the sp2 C–C bonds, N=C–N, and C–O groups induced by unavoidable oxidation, respectively. Additionally, there are three nitrogen species present in the N1s spectrum (Figure S3B) centred at 398.6, 399.6, and 401.1 eV, corresponding to C–N=C, N–$(C)_3$ and C–N–H, respectively. Among them, the ratio of N–$(C)_3$ decreases for D-CN compared with CN. From these observations, we deduce that the aromatic unit of D-CN was more incomplete than CN, in particularly, the broken of cross-linked nitrogen in D-CN might lead to the nitrogen loss and formation of C=O bond, which is in good agreement with the FTIR analysis.

To get further insight into the intrinsic structure of the CN and D-CN, we then examined the C and N K-edge XAENES spectra. Looking at the C K-edge XANES spectra in Figure 2(c), the samples both exhibit two distinct peaks at ~287.9 (A) and ~294 eV (B). The signal A corresponds to the sp2-hybridized carbon in N-containing aromatic rings (N–C=N), which is the major carbon species in the g-C_3N_4 polymer. In addition, its intensity for the D-CN sample is found to be lower than that of bulk CN, indicating the deterioration of crystallinity, reduction of polymerization degree, or defective spatial structure. On the other hand, the feature B is related to interlayer states or transitions to sp3 hybridized states [35].

Figure 2(d) shows the N K-edge XANES spectra of the samples. CN and D-CN both exhibit at least five peaks. The neighbouring peaks a and b at around 399.5 and 400.0 eV can be identified as the unoccupied π^* orbitals in pyridine-like C=N–C bonds and the graphitic-type N, respectively. Both of them, together with sp2 hybridized C (N–C=N), make up the heptazine heterocyclic ring (C_6N_7) units for the construction of the basic substructural units of the g-C_3N_4 polymer. Another two adjacent peaks are centered at 402.6 and 403.0 eV, which are attributable to the amino-type N and the pyrrolic-type N, respectively [36]. Furthermore, a strongly weakened tendency appeared at the D-CN compared with the CN in the σ^* region of the N K-edge (region e), and a 1s $\rightarrow$ σ^* transition is observed as a broad feature centered at ~407 eV which is a superposition of graphite-type N and pyridine-like N structures and sensitive to the bond length between N and C [37].

The N_2 adsorption-desorption isotherms were also investigated, as shown in Figure 3, together with the TEM images (Figure 3, inset). The BET surface area of the D-CN sample is

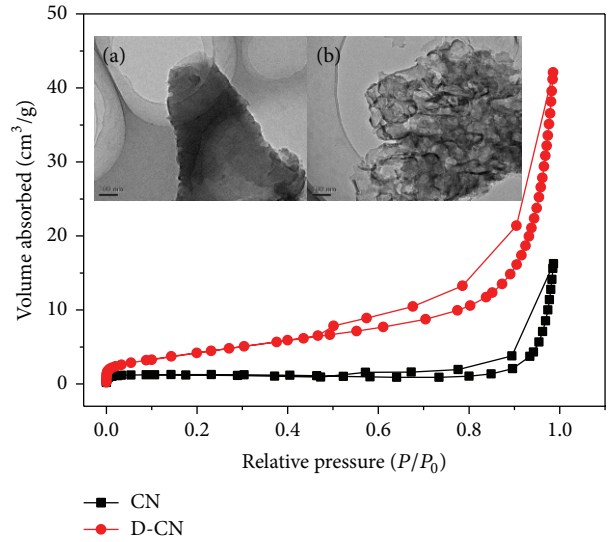

Figure 3: N_2 adsorption-desorption isotherms of CN and D-CN. Inset is the TEM images of (a) CN and (b) D-CN samples.

16.1 $m^2 g^{-1}$, which is almost three times higher than the bulk CN (5.1 $m^2 g^{-1}$). As shown in Figure 3 (inset), the CN displays two-dimensional layered and plate-like sheets, while a much more loose aggregated structure accompanied with some nanosized channels or pores on the surface can be observed for D-CN, indicating the important role of the disordered precursor. This fabricated D-CN with high surface area and unique surface structure could be favourable for improving photocatalytic activity for H_2 evolution, which deserved a further investigation.

The UV-vis spectra are shown in Figure 4(a). Compared with the bulk CN, a remarkable red shift of the optical absorption was observed for D-CN, which suggests a decreased band gap. The characteristic appearing near 500 nm is ascribed to n-π^* transitions which involves lone pairs on the edge N atoms of the triazine/heptazine rings [38]. Furthermore, the transitions cannot appear for the perfectly symmetric C_3N_4 units, and they are observed here as the structures are distorted with the increased defects and holes, including effects from both layer buckling and deviation of the ring units from trigonal symmetry. Consequently, the extension of electron delocalization in the aromatic sheets with enhanced structural connections conduces the shift, somewhat similar to the bathochromic shift effect in J-aggregates. Within this context, more solar photon flux can be covered since the absorbance wavelength range extends to 800 nm. The enhanced absorbance intensities together with the enlarged surface areas are favourable for light harvesting and charge transfer that can improve the photocatalytic performance significantly.

Figure S4 shows the PL spectra of the as-prepared samples excited by 365 nm at room temperature. For these two samples, one main emission peak appears at about 465 nm, ascribed to the band-band recombination of the charge carriers with emission photon energy equal to its bandgap energy. Correspondingly, an obvious fluorescence quenching

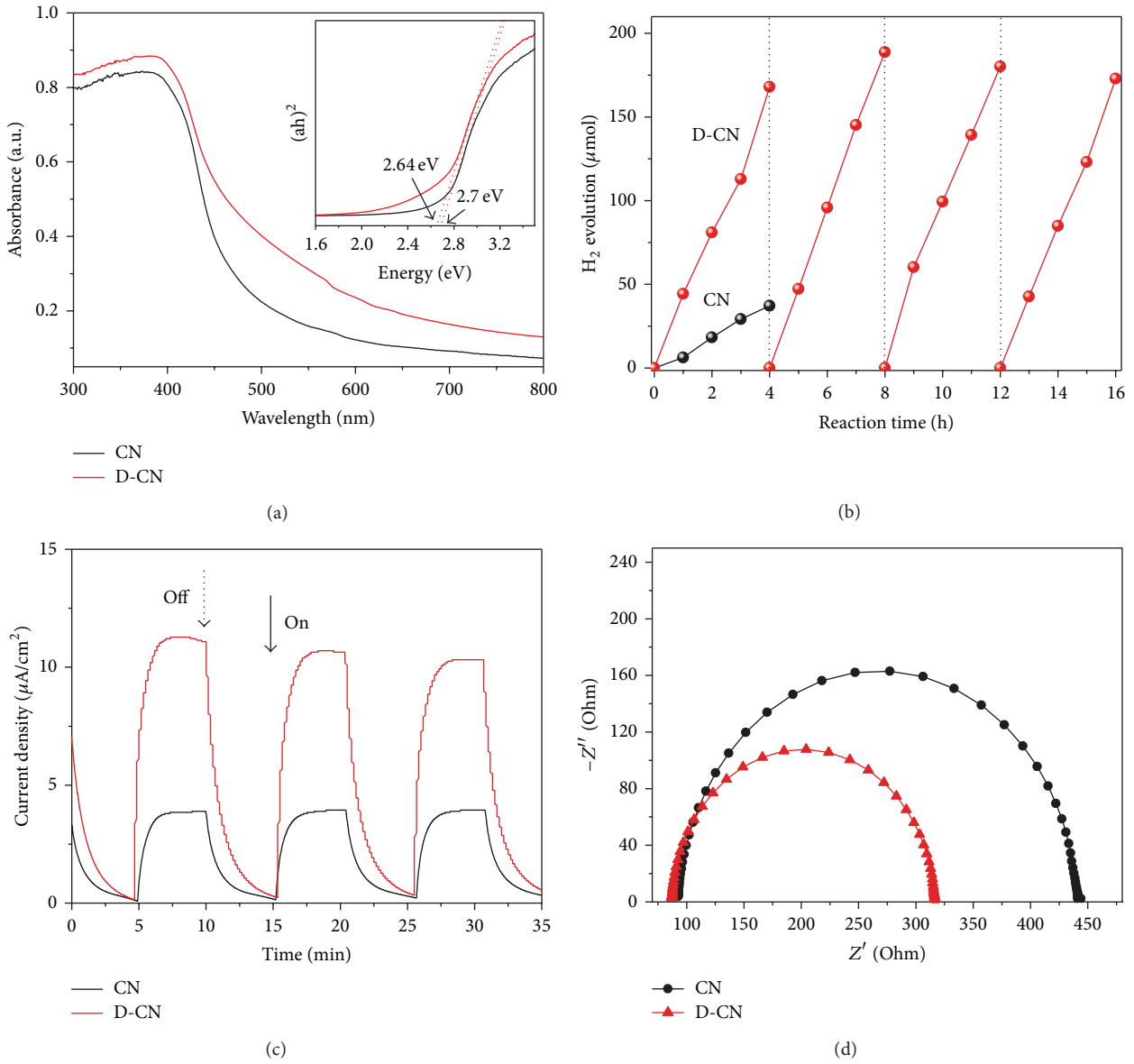

FIGURE 4: (a) UV-vis absorption spectra of the CN and D-CN samples. (b) Stability test of 3.0 wt% Pt-deposited D-CN (50 mg) for H_2 production in aqueous triethanolamine solution (10 vol%) under visible light and CN sample is also shown for comparison. (c) Transient photocurrent generation from CN and D-CN electrodes at 0.6 V versus Ag/AgCl in 0.2 M Na_2SO_4 under simulated sunlight irradiation. (d) EIS Nyquist plots of CN and D-CN.

is observed for the D-CN sample. That means the radiative charge recombination, which happens on the CN sample, has been efficiently suppressed. The suppression is due to the electron relocalization on surface terminal sites or the reduced density of charge carrier traps for electron-hole recombination. Furthermore, radiationless transitions have also been considered to cause fluorescence quenching, which is an unwanted process in photocatalysis either, increasing heat loss [39].

Visible-light-induced hydrogen production was evaluated to examine the catalytic activity of the samples, and a 16 h experiment with intermittent evacuation every 4 h was performed to investigate the stability of D-CN. Figure 4(b) shows a remarkable improvement of D-CN sample in hydrogen evolution activities over bulk CN, whilst it increases steadily without noticeable deterioration of the activity. In addition, an extremely high apparent quantum yield (AQY, 2.7%) is obtained at 420 nm. The turnover numbers with respect to the melem units and Pt atoms are 2.05 and 74.2, respectively, clearly indicating that the reaction indeed proceeds catalytically.

The transient photocurrent responses of the CN and D-CN samples were investigated at a constant voltage of 0.6 V versus Ag/AgCl with several on-off cycles of intermittent simulated sunlight irradiation. As shown in Figure 4(c), both CN and D-CN photoanodes demonstrated steady and prompt

photocurrent generation during the on and off cycles of illumination, manifesting the photoelectrochemical activity and stability of both samples. The D-CN photoanode shows more than two times higher photocurrent intensity than the CN photoanode. To gain deeper insights into the charge transport behaviour in the samples, we also conducted electrochemical impedance spectroscopy (EIS) measurements in dark (Figure 4(d)). The D-CN exhibits the much smaller semicircular in Nyquist plots, suggesting a higher electron transfer conductivity of in D-CN film than in CN film [40]. The calculated electron transfer resistances with an equivalent circuit are 229.9 Ω and 372.3 Ω for the D-CN and CN photoanodes, respectively.

4. Conclusions

In summary, a facile method using disordered precursors was introduced to produce g-C_3N_4 with optimized structures for hydrogen evolution. The loose aggregates which are held together by weak, noncovalent interactions play important roles in living systems and the tiny distinction will influence the traditional chemical route. The final D-CN sample has improved intrinsic texture, morphology, optical properties and therefore leads to a significant enhancement in the photocatalytic activity for hydrogen evolution under visible light. This opens up new dimensions for the study of a general approach for preparing other catalysts with improved or new properties and extended applications.

Conflict of Interests

The authors declare that there is no conflict of interests regarding the publication of this paper.

Acknowledgments

The authors thank Professor Caihao Hong for the valuable discussion on XANES. This work was financially supported by National Natural Science Foundation of China (21373083), SRF for ROCS, SEM, SRFDP, Programme for Professor of Special Appointment (Eastern Scholar) at Shanghai Institutions of Higher Learning and Australian Research Council's Future Fellowships (FT120100913).

References

[1] X. Chen, S. Shen, L. Guo, and S. S. Mao, "Semiconductor-based photocatalytic hydrogen generation," *Chemical Reviews*, vol. 110, no. 11, pp. 6503–6570, 2010.

[2] A. Fujishima and K. Honda, "Electrochemical photolysis of water at a semiconductor electrode," *Nature*, vol. 238, no. 5358, pp. 37–38, 1972.

[3] Z. Yi, J. Ye, N. Kikugawa et al., "An orthophosphate semiconductor with photooxidation properties under visible-light irradiation," *Nature Materials*, vol. 9, no. 7, pp. 559–564, 2010.

[4] X. Wang, K. Maeda, A. Thomas et al., "A metal-free polymeric photocatalyst for hydrogen production from water under visible light," *Nature Materials*, vol. 8, no. 1, pp. 76–80, 2009.

[5] A. Thomas, A. Fischer, F. Goettmann et al., "Graphitic carbon nitride materials: variation of structure and morphology and their use as metal-free catalysts," *Journal of Materials Chemistry*, vol. 18, no. 41, pp. 4893–4908, 2008.

[6] I. D. W. Samuel and G. A. Turnbull, "Organic semiconductor lasers," *Chemical Reviews*, vol. 107, no. 4, pp. 1272–1295, 2007.

[7] G. Liu, P. Niu, C. Sun et al., "Unique electronic structure induced high photoreactivity of sulfur-doped graphitic C_3N_4," *Journal of the American Chemical Society*, vol. 132, no. 33, pp. 11642–11648, 2010.

[8] J. Li, B. Shen, Z. Hong, B. Lin, B. Gao, and Y. Chen, "A facile approach to synthesize novel oxygen-doped g-C_3N_4 with superior visible-light photoreactivity," *Chemical Communications*, vol. 48, no. 98, pp. 12017–12019, 2012.

[9] B. Yue, Q. Li, H. Iwai, T. Kako, and J. Ye, "Hydrogen production using zinc-doped carbon nitride catalyst irradiated with visible light," *Science and Technology of Advanced Materials*, vol. 12, no. 3, Article ID 034401, 2011.

[10] Z. Lin and X. Wang, "Nanostructure engineering and doping of conjugated carbon nitride semiconductors for hydrogen photosynthesis," *Angewandte Chemie—International Edition*, vol. 52, no. 6, pp. 1735–1738, 2013.

[11] H. Yan, "Soft-templating synthesis of mesoporous graphitic carbon nitride with enhanced photocatalytic H_2 evolution under visible light," *Chemical Communications*, vol. 48, no. 28, pp. 3430–3432, 2012.

[12] X. Wang, K. Maeda, X. Chen et al., "Polymer semiconductors for artificial photosynthesis: hydrogen evolution by mesoporous graphitic carbon nitride with visible light," *Journal of the American Chemical Society*, vol. 131, no. 5, pp. 1680–1681, 2009.

[13] X.-H. Li, J. Zhang, X. Chen et al., "Condensed graphitic carbon nitride nanorods by nanoconfinement: promotion of crystallinity on photocatalytic conversion," *Chemistry of Materials*, vol. 23, no. 19, pp. 4344–4348, 2011.

[14] Y. Hou, A. B. Laursen, J. Zhang et al., "Layered nanojunctions for hydrogen-evolution catalysis," *Angewandte Chemie: International Edition*, vol. 52, no. 13, pp. 3621–3625, 2013.

[15] Y. Di, X. Wang, A. Thomas, and M. Antonietti, "Making metal-carbon nitride heterojunctions for improved photocatalytic hydrogen evolution with visible light," *ChemCatChem*, vol. 2, no. 7, pp. 834–838, 2010.

[16] J. Zhang, G. Zhang, X. Chen et al., "Co-monomer control of carbon nitride semiconductors to optimize hydrogen evolution with visible light," *Angewandte Chemie*, vol. 51, no. 13, pp. 3183–3187, 2012.

[17] J. Zhang, X. Chen, K. Takanabe et al., "Synthesis of a carbon nitride structure for visible-light catalysis by copolymerization," *Angewandte Chemie*, vol. 49, no. 2, pp. 441–444, 2010.

[18] A. Suryawanshi, P. Dhanasekaran, D. Mhamane et al., "Doubling of photocatalytic H_2 evolution from g-C_3N_4 via its nanocomposite formation with multiwall carbon nanotubes: electronic and morphological effects," *International Journal of Hydrogen Energy*, vol. 37, no. 12, pp. 9584–9589, 2012.

[19] Q. Li, B. Yue, H. Iwai, T. Kako, and J. Ye, "Carbon nitride polymers sensitized with N-doped tantalic acid for visible light-induced photocatalytic hydrogen evolution," *The Journal of Physical Chemistry C*, vol. 114, no. 9, pp. 4100–4105, 2010.

[20] X. L. Wang, W. Q. Fang, H. F. Wang et al., "Surface hydrogen bonding can enhance photocatalytic H_2 evolution efficiency," *Journal of Materials Chemistry A*, vol. 1, no. 45, pp. 14089–14096, 2013.

[21] X. L. Wang, W. Q. Fang, S. Yang, P. Liu, H. Zhao, and H. G. Yang, "Structure disorder of graphitic carbon nitride induced by liquid-assisted grinding for enhanced photocatalytic conversion," *RSC Advances*, vol. 4, no. 21, pp. 10676–10679, 2014.

[22] Y. Cui, J. Zhang, G. Zhang et al., "Synthesis of bulk and nanoporous carbon nitride polymers from ammonium thiocyanate for photocatalytic hydrogen evolution," *Journal of Materials Chemistry*, vol. 21, no. 34, pp. 13032–13039, 2011.

[23] F. Dong, L. Wu, Y. Sun, M. Fu, Z. Wu, and S. C. Lee, "Efficient synthesis of polymeric g-C_3N_4 layered materials as novel efficient visible light driven photocatalysts," *Journal of Materials Chemistry*, vol. 21, no. 39, pp. 15171–15174, 2011.

[24] F. Dong, Y. Sun, L. Wu, M. Fu, and Z. Wu, "Facile transformation of low cost thiourea into nitrogen-rich graphitic carbon nitride nanocatalyst with high visible light photocatalytic performance," *Catalysis Science and Technology*, vol. 2, no. 7, pp. 1332–1335, 2012.

[25] G. R. Desiraju, "Linus Pauling: the all-chemist," *Nature*, vol. 408, no. 6811, p. 407, 2000.

[26] G. R. Desiraju, "Chemistry beyond the molecule," *Nature*, vol. 412, no. 6845, pp. 397–400, 2001.

[27] T. Steiner, "The hydrogen bond in the solid state," *Angewandte Chemmie—International Edition*, vol. 41, pp. 48–76, 2002.

[28] E. Boldyreva, "Mechanochemistry of inorganic and organic systems: what is similar, what is different?" *Chemical Society Reviews*, vol. 42, no. 18, pp. 7719–7738, 2013.

[29] E. W. Hughes, "The crystal structure of dicyandiamide," *Journal of the American Chemical Society*, vol. 62, no. 5, pp. 1258–1267, 1940.

[30] W. J. Jones and W. J. Orville-Thomas, "The infra-red spectrum and structure of dicyandiamide," *The Faraday Society and Contributors*, vol. 55, pp. 193–202, 1959.

[31] F. Dong, M. Ou, Y. Jiang, S. Guo, and Z. Wu, "Efficient and durable visible light photocatalytic performance of porous carbon nitride nanosheets for air purification," *Industrial and Engineering Chemistry Research*, vol. 53, no. 6, pp. 2318–2330, 2014.

[32] K. Parvez, S. Yang, Y. Hernandez et al., "Nitrogen-doped graphene and its iron-based composite as efficient electrocatalysts for oxygen reduction reaction," *ACS Nano*, vol. 6, no. 11, pp. 9541–9550, 2012.

[33] Y. Hou, Z. Wen, S. Cui, X. Guo, and J. Chen, "Constructing 2D porous graphitic C_3N_4 nanosheets/nitrogen-doped graphene/layered MoS_2 ternary nanojunction with enhanced photoelectrochemical activity," *Advanced Materials*, vol. 25, no. 43, pp. 6291–6297, 2013.

[34] J.-B. Zhang, Z.-C. Tan, S.-H. Meng, S.-H. Li, and L.-M. Zhang, "Heat capacity and thermal decomposition of dicyandiamide," *Thermochimica Acta*, vol. 307, no. 1, pp. 11–15, 1997.

[35] L. Liu, T.-K. Sham, and W. Han, "Investigation on the electronic structure of BN nanosheets synthesized via carbon-substitution reaction: The arrangement of B, N, C and O atoms," *Physical Chemistry Chemical Physics*, vol. 15, no. 18, pp. 6929–6934, 2013.

[36] Y. Gao, G. Hu, J. Zhong et al., "Nitrogen-doped sp2-hybridized carbon as a superior catalyst for selective oxidation," *Angewandte Chemie*, vol. 52, no. 7, pp. 2109–2113, 2013.

[37] S. C. Ray, C. W. Pao, J. W. Chiou et al., "Electronic properties of a-CN_x thin films: an x-ray-absorption and photoemission spectroscopy study," *Journal of Applied Physics*, vol. 98, no. 3, Article ID 033708, 2005.

[38] A. B. Jorge, D. J. Martin, M. T. S. Dhanoa et al., "H_2 and O_2 evolution from water half-splitting reactions by graphitic carbon nitride materials," *Journal of Physical Chemistry C*, vol. 117, no. 14, pp. 7178–7185, 2013.

[39] J. Zhang, M. Zhang, R.-Q. Sun, and X. Wang, "A facile band alignment of polymeric carbon nitride semiconductors to construct isotype heterojunctions," *Angewandte Chemie—International Edition*, vol. 51, no. 40, pp. 10145–10149, 2012.

[40] Y. Hou, F. Zuo, A. Dagg, and P. Feng, "A three-dimensional branched cobalt-doped α-Fe_2O_3 nanorod/$MgFe_2O_4$ heterojunction array as a flexible photoanode for efficient photoelectrochemical water oxidation," *Angewandte Chemie—International Edition*, vol. 52, no. 4, pp. 1248–1252, 2013.